Egypt. J. Chem. **Vol. 68**, No. 3. pp. 479 - 491 (2025)

Egyptian Journal of Chemistry

http://ejchem.journals.ekb.eg/

A Comparative Study on Synthesis and Characterization of Hydroxyapatite Nanoparticles from Different Industrial and Bio-Wastes

Maher M. Girgis[1], Nady A. Fathy[*2], Mostafa Farrag[1], Mohammed A. Elnahas[1],

[1)] Chemistry Department, Faculty of Science, Assiut University, P.O. 71515, Assiut, Egypt

[2)]Physical Chemistry Department, Advanced Materials Technology and Mineral Resources Research Institute, National Research Centre, 33 EL Buhouth St., Dokki, Cairo, P.O. 12622, Egypt

Abstract

Hydroxyapatite (HAP), as a bioceramic substance, has a wide range of research and application opportunities in materials science and biomedicine. This study spotlights the feasibility production of sustainable HAPs from diverse waste sources to showcasing their potential utilities for environmentally friendly applications and reduced ecological impacts. Thus, cement kiln dust (CKD), eggshell and buffalo bone wastes were applied for preparing main HAP precursors such as calcium sulfate, calcium nitrate and non pure HAP in bone, respectively. During reaction of diammonium hydrogen phosphate ($(NH_4)_2HPO_4$) with extracted calcium sulfate; HAP samples were obtained via microwave and hydrothermal routes. Chemical precipitation route was performed in case of calcium nitrate extracted from eggshell to prepare aHAP. Non pure HAP in bone was treated by three methods; i.e., subcritical water process, alkaline hydrothermal hydrolysis and thermal decomposition to produce pure HAP samples. Characterization of HAP obtained was performed using XRD, FTIR, XPS, TGA, N_2 adsorption-desorption at -196^{o}C and SEM analyses. Porous HAP samples were successfully prepared using $CaSO_4$-CKD and $Ca(NO_3)_2$-eggshell with rough surfaces composed of spherical particles and high total surface areas (93.8-150.3 m^2/g), whereas HAP obtained from buffalo bone exhibited the lowest porosity (12.9-34 m^2/g). The prepared samples outperformed the purchased HAP sample in terms of surface and textural qualities, with a Ca/p ratio of around 1.66, comparable to natural HAP.Conclusively, the calcium supplies derived from CKD and eggshells are superior precursors to produce highly porous HAP samples than calcium sources derived from buffalo bones.

Keywords:Hydroxyapatite, cement kiln dust, eggshell, buffalo bone, characterizations

1. Introduction

Today, the waste from natural sources is a useful resource for extracting and recovering valuable substances. The conversion of these waste products into valuable materials using specialized procedures and approaches is one of these attempts [1]. As calcium-phosphate-based bioceramic materials, hydroxyapatite (HAP, $Ca_{10}(OH)_2(PO)_6$) with molar ratio of Ca/P = 1.67 is the primary inorganic component of bone and teeth and provides them their high stability, hardness and function. Hence, it is extremely important in the biomedical sector and tissue engineering applications [1, 2]. HAP is a naturally occurring mineral with notable characteristics, including biocompatibility, water insolubility, thermal and chemical stability and structural flexibility [3]. Its highly functionalized surface features both acidic and basic groups, making it amphoteric and enabling a wide range of applications, ranging from biomedicine to catalysis [3]. Its surface properties showed promising outcomes, signifying the potential importance of HAP in various domains [4]. These exceptional attributes have captured the attention of researchers to make extensive investigations on the synthesis of HAP from low-cost wastes. HAP may be produced using inexpensive and easily accessible mostly Ca-based minerals[5-15]. Among these sources, gypsum [5] and biological wastes such as animal bones[6], Fish scales[7] and eggshells [8]were utilized. There are several HAP preparation techniques, which may be divided into dry and wet preparation routes. The term "dry preparation" most often refers to the solid-phase reaction preparation between raw material powders (*e.g.* $CaHPO_4$ and CaO) via techniques such as thermal treatment, mechanochemical and plasma spray [9]. Contrarily, there are a variety of wet preparation techniques, including chemical precipitation [10], hydrothermal [11], microemulsion[12], calcination [13] and sol-gel [14].

To achieve sustainability and efficiency, there is a growing emphasis on using industrial by-products and bio-waste as raw materials for nano-HAP synthesis. This approach mitigates environmental impacts and introduces unique functionalities, expanding the potential applications. In this study, three different calcium-based sources of HAP from

*Corresponding author e-mail: fathyna.77@hotmail.com,. (Nady A. Fathy).

Received date 20 June 2024; Revised date 14 July 2024; Accepted date 30 July 2024

DOI: 10.21608/EJCHEM.2024.298292.9879

industrial and biological wastes, including cement kiln dust (CKD), egg shells and Buffalo bone were employed and investigated.

The cement industry generates substantial amounts of hazardous waste known as CKD, which poses risks to ecosystems and organisms due to its alkalinity and heavy metal concentration [15]. The CEMEX cement plant near Assiut City in Upper Egypt is a substantial contributor to CKD generation. For every ton of cement clinker produced, a significant amount of CKD, ranging from 54 to 200 kg, is generated [16]. Research in this area aims to propose effective strategies and protocols for managing industrial waste, mitigating environmental pollution and achieving a balance between environmental preservation and resource utilization through waste recycling. Therefore, the current study also explores the economic potential of harnessing CKD, as a potentially hazardous byproduct, to produce valuable resources like HAP, thus mitigating the cement industry's environmental footprint [17]. For eggshell utilization, chicken eggshells mainly consist of calcium carbonate ($CaCO_3$, 94%), calcium phosphate (1%), organic matter (4%) and magnesium carbonate (1%). The choice of eggshells as a resource is driven by their high calcium content, making them suitable for the synthesis of HAP [18]. For bone utilization, bones compose of 30% organics and 70% inorganics with a mineral phase consisting a nonstoichiometric HAP, which has a variable Ca/P molar ratio (less or more than 1.67) and additional minerals, including Fe^{2+}, Na^{2+}, Mg^{2+}, Zn^{2+}, Si^{2+}, Ba^{2+} and CO_3^{-2} [19]. Extraction of a stoichiometric bioactive HAP from animal bones is a crucial challenge where its bioactivity is largely influenced by the proportion of calcium, phosphate (Ca/P)[19]. In general, few methods of extracting hydroxyapatite from animal bones such as thermal decomposition, subcritical water process and alkaline hydrolysis have been studied [20, 21]. The current work is aimed to investigate the feasible preparation of HAP nanoparticles from calcium-based local wastes that disposed in large quantities such as cement kiln dust (CKD), eggshells and buffalo bones under different methods. The following tools such as X-ray diffraction (XRD), Fourier transform infrared (FTIR) spectroscopy, X-ray photoelectron spectroscopy (XPS), thermogravimetric (TG), N_2 adsorption-desorption at -196ºC and scanning electron microscope (SEM) analyses were all used to examine the final properties of synthesized HAP compared with the purchased commercial HAP.

2. Materials and Methods

2.1. Materials

A specimen of grayish-green *Cement Kiln Dust* (CKD) was procured from the CEMEX cement Plant situated in the Assiut Governorate of Egypt. Eggshells were sourced from a local poultry farm, in Assiut. Buffalo bones were procured from a local abattoir, Assiut.Di-ammonium hydrogen orthophosphate ($(NH_4)_2HPO_4$, 97%, ADWIC), ammonium hydroxide (NH_4OH, 25% NH3, ADWIC),sodium hydroxide (NaOH, 96%, ADWIC),trisodium citrate ($C_6H_5Na_3O_7$, 98%, United chemical laboratory), sulfuric acid (H_2SO_4,95-97%, Riedel-de Haën), nitric acid (HNO_3,65%, Riedel-de Haën) and acetone (CH_3COCH_3, 99.8%, PIOCHEM). A commercial HAP (97%, Sigma-Aldrich) was used to confirm the formation of HAP from selected wastes such as CKD, eggshells and buffalo bones via different techniques.

2.2. Preparation of Hydroxyapatite from Cement Kiln Dust (CKD)

To attain this objective, calcium sulfate as HAP precursor was extracted from CKD through two steps after thorough washing with distilled water to reduce other impurities. The CKD's chemical composition underwent analysis was detected via X-ray fluorescence (XRF) by NITON XLP 300A/700A series. The resultant data is displayed in Table 1.

Table 1: Chemical composition of CKD raw material

Compound or Element	SiO_2	Al_2O_3	Fe_2O_3	CaO	MgO	SO_3	Na_2O	K_2O	Cl
wt %	11.51	3.07	2.40	40.99	0.62	15.22	5.24	6.88	7.54

The CKD underwent dual washes employing distilled/de-ionized water to eliminate impurities, followed by filtration. After filtration, the sample was subjected to drying at 110°C throughout one night. The ensuing dried CKD powder was subjected to a calcium elution process using a 0.1M trisodium citrate (TSC) as a chelating agent at a ratio of 1 g CKD to 50 ml TSC [22] in order to extract calcium. The mixture underwent mechanical stirring for one hour, after which the eluate was filtered using filter paper No. 41. This elution process was reiterated to ensure thorough calcium removal from CKD. In the subsequent step, the elution calcium citrate complex solution was treated with 0.1M H_2SO_4 solution to until the pH stabilized at 6.5 for the production of calcium sulfate ($CaSO_4$) [23]. The ensuing solution was subjected to evaporation to remove excess water, thereby white precipitating $CaSO_4$ was obtained. This precipitate was subsequently washed with distilled water and dried at 105°C overnight. The synthesis of HAP from $CaSO_4$ precursor derived from CKD was pursued through two methods including microwave and hydrothermal as follows.

2.2.1. Microwave synthesis of Hydroxyapatite from $CaSO_4$

The obtained $CaSO_4$ (10 grams) was amalgamated with 400 ml of 1 M diammonium hydrogen phosphate ($(NH_4)_2HPO_4$) within a Pyrex glass flask [24]. The solution was subjected to microwave irradiation (multimode microwave oven (MILSTONE START SYNTH 1200 W/ 2450 MHZ)) for 20 minutes at 800 watts. The obtained HAP powder was cleansed with distilled water and dried at 105ºC overnight.

2.2.2. Hydrothermal synthesis of Hydroxyapatite from $CaSO_4$

A mixture comprising 40 ml of 1M $(NH_4)_2HPO_4$ and 4 grams of $CaSO_4$ was confined within a stainless-steel autoclave housed within a Teflon crucible [25]. The mixture was elevated to a temperature of 120°C for 6 hours. The resultant HAP powder underwent cleansing with distilled water and subsequent drying at 105ºC overnight.

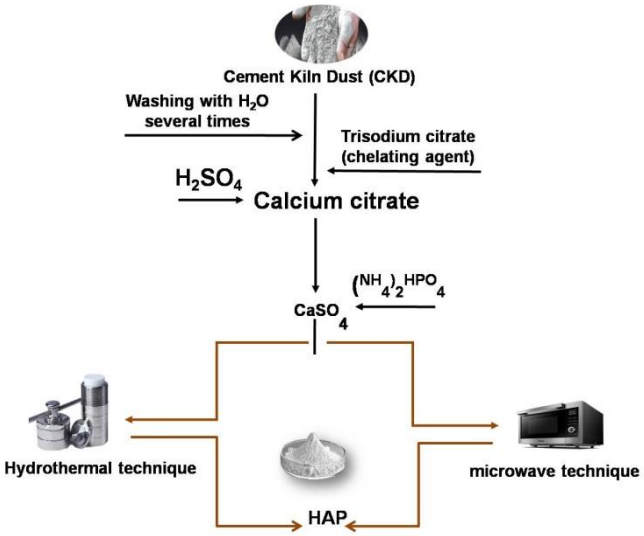

Scheme 1: Chart-flow for synthesis of HAP from CKD waste.

2.3. Preparation of Hydroxyapatite from Eggshells

Preparation of HAP from eggshell wastes was carried out according to the procedure described by Mobarak et al. [26]. Eggshells were washed with distilled water to eliminate observable impurities and dried at 80°C overnight. Post-drying, the eggshells were pulverized using a ball mill to attain a finely powdered state. Acetone was employed to eliminate any residual organic matter. Calcium nitrate ($Ca(NO_3)_2$) was produced using 7.7 M HNO_3 at a ratio of 1 g eggshells to 3 ml HNO_3, followed by drying at 105°C for 24 hours. Calcium nitrate served as the exclusive source of calcium ions, while diammonium hydrogen phosphate provided the phosphate source. The required quantities of calcium nitrate and diammonium hydrogen phosphate were dissolved in distilled water, with aqueous ammonia (28–30% assay) incorporated to maintain a stable pH of 11. The synthesis of HAP was executed at a temperature of 37°C to promote the growth of nanophase HAP crystals [27]. In brief, solutions of $Ca(NO_3)_2$ (0.4 M) and $(NH_4)_2HPO_4$ (0.239 M) were prepared and subjected to continuous stirring for two hours at a rate of 350 RPM on a thermal magnetic stirrer at 30°C. This temperature facilitated complete salt dissolution. The calcium nitrate solution was accommodated within a flask on a magnetic stirrer, while the phosphate solution was contained in a burette. The synthesis process was initiated with a stirring temperature of 37°C when the phosphate solution was introduced drop-wise at a rate of 3 ml/min. Adjustment of pH to 11 was conducted using aqueous ammonia. The culmination of the reaction yielded a dense yellowish-white precipitate which was stirred overnight, rinsed with deionized water and air-dried at 105ºC overnight. The fundamental reaction and synthesis of HAP are represented as follows:

$$\mathbf{10\ Ca(NO_3)_2 + 6\ (NH_4)_2HPO_4 + 8\ NH_4OH \rightarrow Ca_{10}(PO_4)_6(OH)_2 + 20\ NH_4NO_3 + 6\ H_2O.}$$

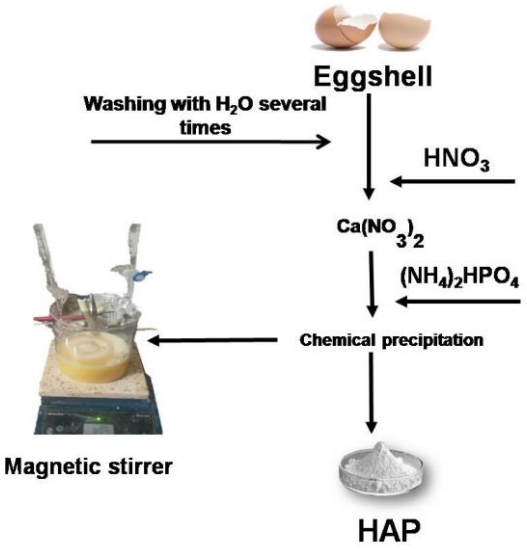

Scheme 2: Chart-flow for synthesis of HAP from eggshell waste.

2.4. Preparation of Hydroxyapatite from buffalo *Bone*

Due to buffalo bones contain non-pure HAP, thus bones were subjected to different treatments after thorough cleaning with distilled water and acetone to eliminate discernible impurities and then sterilized at 200°C for 5 hours [20]. The sterilized bones were crushed and finely ground using a ball mill and sieved to obtain a fine powder with particles measuring less than 500 micrometers. Acetone was utilized to remove any remaining organic matter from the powder. The ensuing white powder underwent cleaning with distilled water and drying at 110°C for 24 hours. The synthesis of HAP from bone encompassed three routes: subcritical water process, alkaline hydrothermal hydrolysis and thermal decomposition as reported elsewhere [19, 20, 28].

2.4.1. Subcritical Water Process
Buffalo bone powder was mixed with deionized water at a weight ratio of 1:40 and introduced into a cylindrical hydrothermal stainless-steel autoclave equipped with a Teflon crucible. The autoclave was sealed and the mixture was subjected to heating for one hour at 275°C. Post-cooling, the mixture was filtered and the HAP obtained was rinsed with deionized water before drying at 80°C for 30 minutes.
2.4.2. Alkaline Hydrothermal Hydrolysis
Buffalo bone powder underwent hydrolysis utilizing a 25-weight percent sodium hydroxide solution at a solid-to-liquid weight ratio of 1:40. The mixture was transferred into a cylindrical hydrothermal stainless-steel autoclave equipped with a Teflon crucible and then subjected to heating at 250°C for five hours.

2.4.3. Thermal Decomposition
Buffalo bone powder (3 g) was heated at 750°C within an open porcelain crucible at a rate of 10°C/min and maintained for 6 hours. The resulting hydroxyapatite derived from each method underwent washing with distilled water and subsequent air-drying at 80°C overnight.

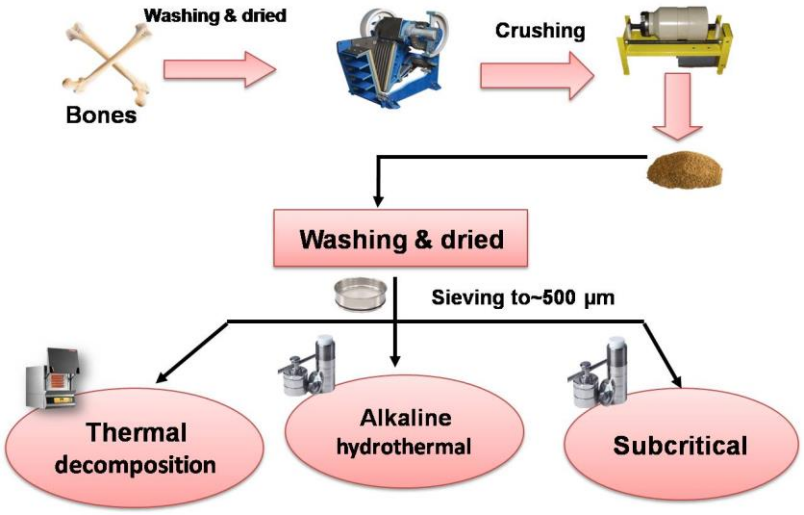

Scheme 3: Chart-flow for synthesis of HAP from bone waste.

2.5. Characterization of Samples
Analyzing the crystallographic phase of HAP involves employing a Philips 1700 version diffractometer with CuKa radiation to acquire XRD patterns within the 2θ range of 4° to 80°. Further scrutiny of functional groups in pure HAP involves Fourier transform infrared (FTIR) spectroscopy within the range of 4000 to 400 cm^{-1}, utilizing the KBr pellet technique and a Nicolet spectrophotometer, model 6700. X-ray photoelectron spectroscopy (XPS) with a monochromatic X-ray Al K-alpha source (Termo Fisher) was meticulously to examine the surface electronic structure and chemical states of HAP.
To determine the thermal behavior of HAP samples, thermogravimetric (TG) and differential thermal analyses (DTA) were studied using a Shimadzu thermal analyzer (Japan, 60H) using N_2 as a heating atmosphere and a heating rate of 10 °C/min to 800°C. Textural characteristics of the samples like specific surface area, total pore volume and average pore radius were determined through N_2 adsorption-desorption isotherm analysis at 77 K using the Brunauer-Emmett-Teller (BET) and Barrett-Joyner-Halenda (BJH) methods using Nova 3200 Multi station High speed Gas sorption analyzer (Quanta-chrome Instrument Corporation, USA). To scrutinize the surface morphology of HAP a scanning electron microscope (SEM) using JSM-5400

LV (Joel, Tokyo, Japan) was used after a coating process with a gold-palladium alloy and mounting on a copper holder, was performed.

3. Results and Discussion

3.1. Crystal phase investigation

The X-ray Diffraction (XRD) patterns of HAP samples synthesized from diverse sources involving three distinct calcium-based resources such as Cement Kiln Dust (CKD), eggshells and buffalo bone using various methods were detected. To comprehensively analyze the XRD patterns, each synthesized HAP sample will be compared with a commercial HAP sample. The individual diffraction patterns are representative of formation of hydroxyapatite and are denoted by (o) as shown in Fig.1 for HAP obtained from CKD, Fig. 2 for HAP prepared from eggshells and Fig. 3 for HAP extracted from the bone. The XRD patterns revealed the prominent peaks corresponding to the hydroxyapatite phases of 2θ values at 25.8°, 31.7°, 34.05°, 39.8°, 46.7°, 49.5° and 53.1° according to (JCPDS card no. 72-1243) [29, 30]. The diffraction pattern intensity is affected by the HAP precursor, method of preparation and reaction or calcination temperature applied. The method and temperature conditions employed in the preparation of commercial HAP are unknown, which could explain why the intensity of their patterns differs from that of synthesized HAP in the current investigation. However, using hydrothermal and microwave techniques to prepare HAP from $CaSO_4$ extracted from CKD precursor resulted in the development of HAP with a semi-amorphous structure due to peak broadening, implying that their particle sizes are nanoscale. An additional result was observed that the XRD patterns of HAP produced from hydrothermal process appeared more reduced in intensity compared to the XRD peaks of HAP obtained through microwave process. The same XRD patterns were obtained for HAP prepared from $Ca(NO_3)_2$ which was extracted from eggshells via chemical precipitation reaction at 37°C [26, 27] as shown in Fig. 2, revealing XRD patterns with higher intensity than those obtained for HAP samples prepared from $CaSO_4$/CKD either by microwave or hydrothermal process.

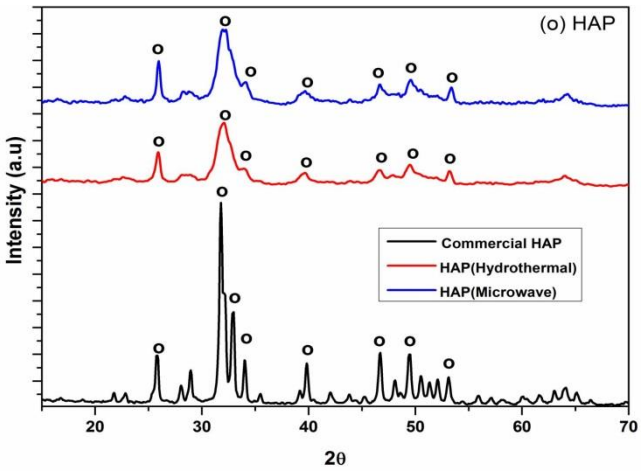

Fig. 1: XRD patterns of HAP samples synthesized from $CaSO_4$ extracted from CKD.

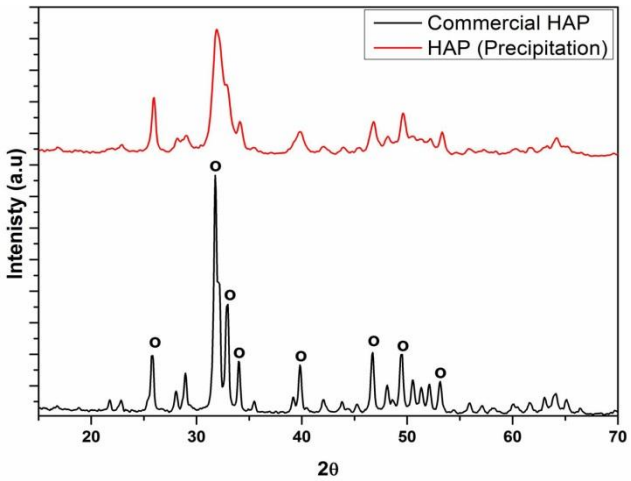

Fig. 2: XRD patterns of HAP samples synthesized from Ca $(NO_3)_2$ extracted from eggshells at 37°C.

Since the chemical composition of Buffalo bone contains calcium and phosphate in the form of a nonstoichiometric HAP, thus three direct methods such as subcritical water hydrothermal, alkaline hydrothermal and thermal decomposition were applied without adding $(NH_4)_2HPO_4$according to previous work by others [20]. Thus, almost all XRD patterns of the HAP samples were analogous to XRD patterns for commercial HAP. As a result, HAP obtained from the thermal decomposition of bone has a well-crystalline structure and closely matched with peaks in commercial HAP as depicted in Fig. 3. From this observation, the intensity of the XRD pattern was increased with increasing temperature indicating the higher crystallinity of HAP obtained via thermal decomposition of Buffalo bone. On the other hand, employing subcritical water and alkaline hydrothermal methods produced semi-amorphous HAP samples like that obtained from CKD-derived $CaSO_4$ and calcium nitrate of eggshells. These results are consistent with data published elsewhere [26, 29]. According to similar results reported by others [31, 32], the XRD patterns of the prepared HAP mostly exhibited three main planes (002), (211) and (300) as the main growth planes of HAP crystals at 2θ= 25.8º, 31.7º and 34.05º. It can be observed that XRD peaks for β-tricalcium phosphate $(Ca_3(PO_4)_2)$ with two diffraction peaks at 30.1º (012) and 33.4º (110) as well as a single diffraction peak related to the presence of $Ca(OH)_2$ at 36.6º (002) were not detected in the XRD profile of HAP samplesprepared from $CaSO_4$, $Ca(NO_3)_2$ and bone sources. Notably, no other crystalline species were detected in the synthesized hydroxyapatite samples, concluding that the obtained HAP is extremely pure. The crystallite size (L) for different samples was calculated from the Scherrer equation [33] which is given by L= Kλ / β cos θ, K represents broadening constant which was taken as 0.9, λ the wavelength of monochromatic X-ray beam (λ = 1.5418Å for CuKα radiation), β is the full-width half maximum (FWHM) and the diffraction angle (θ) and the result represented in Fig, 4. It is clear that the crystallite sizes of HAP prepared varied from 13 to 23.4 nm while is 19.7 nm for the purchased HAP.

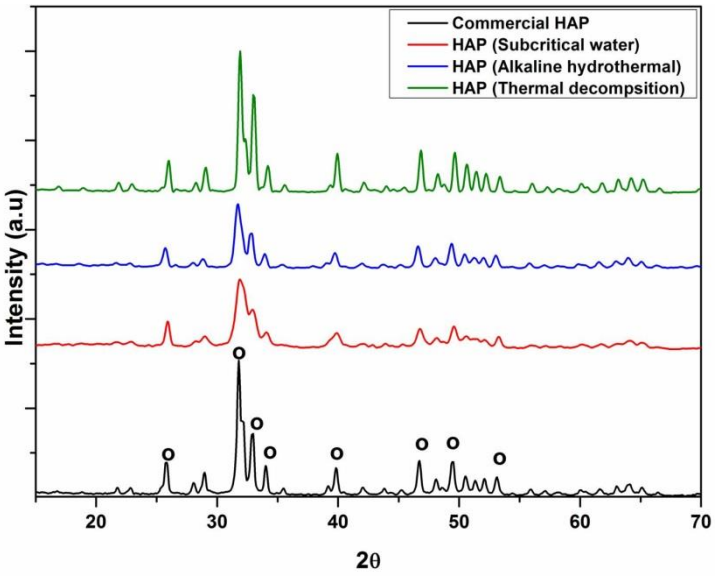

Fig. 3: XRD patterns of HAP samples synthesized from Buffalo bone waste.

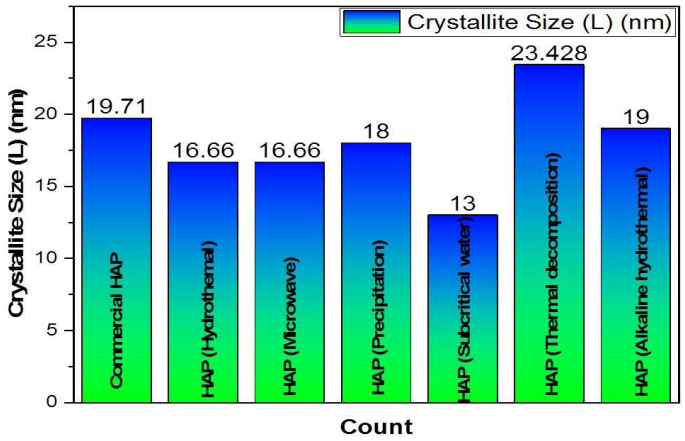

Fig. 4: Crystallite Size (L) (nm) of HAP samples calculated by Scherrer equation.

Recently, Osuchukwu et al. [34] studied the preparation of HAP from animal bones through carbonization, calcination followed by sol-gel. XRD results of the obtained HAP showed crystallite sizes between 24 and 25.4 nm which are larger than that of HAP produced from buffalo bones in this study (13-23 nm), confirming the successful preparation of HAP under the prescribed methods.

3.2. Functional groups identified by FTIR

Fig. 5 shows the FTIR spectra of all HAP samples in comparison with that of commercial HAP. In our study, three calcium salts of $CaSO_4$, Ca $(NO_3)_2$ and calcium-based bone were extracted from CKD, eggshells and Buffalo bone, respectively. To obtain HAP, current methods such as hydrothermal and microwave were carried out using $CaSO_4$ from CKD, chemical precipitation was applied in case of Ca $(NO_3)_2$ from eggshells, whereas as subcritical water hydrothermal, alkaline hydrothermal and thermal decomposition were used directly with Buffalo bone. All characteristics surface functional groups such as (OH^-), $(PO_4)^{3-}$ and CO_3^- which are related to $Ca_{10}(OH)_2(PO)_6$, are detected in all studied samples using the FTIR tool. Absorption peaks that corresponded to O-H vibration are appeared as broad band at 3457.3 cm^{-1} and shoulder at 1628 cm^{-1}. For phosphate groups, absorption broad band at 1054.1–1065.7 cm^{-1} and two joint shoulder bands at 607.8 and 584.8 cm^{-1} are observed. Smaller bands observed in the range between 1405-1425 cm^{-1} and 865.4–877.5 cm^{-1} are ascribed to (CO_3^-) vibration which are increased in the commercial HAP sample. Additionally, the appearance of a smaller peak at 3575.8 cm^{-1} in the commercial HAP and HAP samples obtained from eggshells-based $Ca(NO_3)_2$ and bone maybe correspond to N-H vibration as a result of N residues in a nitrate or proteins in bones [26, 28]. Two further absorption peaks at 2942.5 and 2848.1 cm^{-1} appeared in HAP obtained from bones via subcritical water and alkaline hydrothermal that attributed to C-H vibration [29] resulting in organics of bones which are fully diminished at elevated temperature between 900-1100^{o}C as reported by Khoo et al. [28].

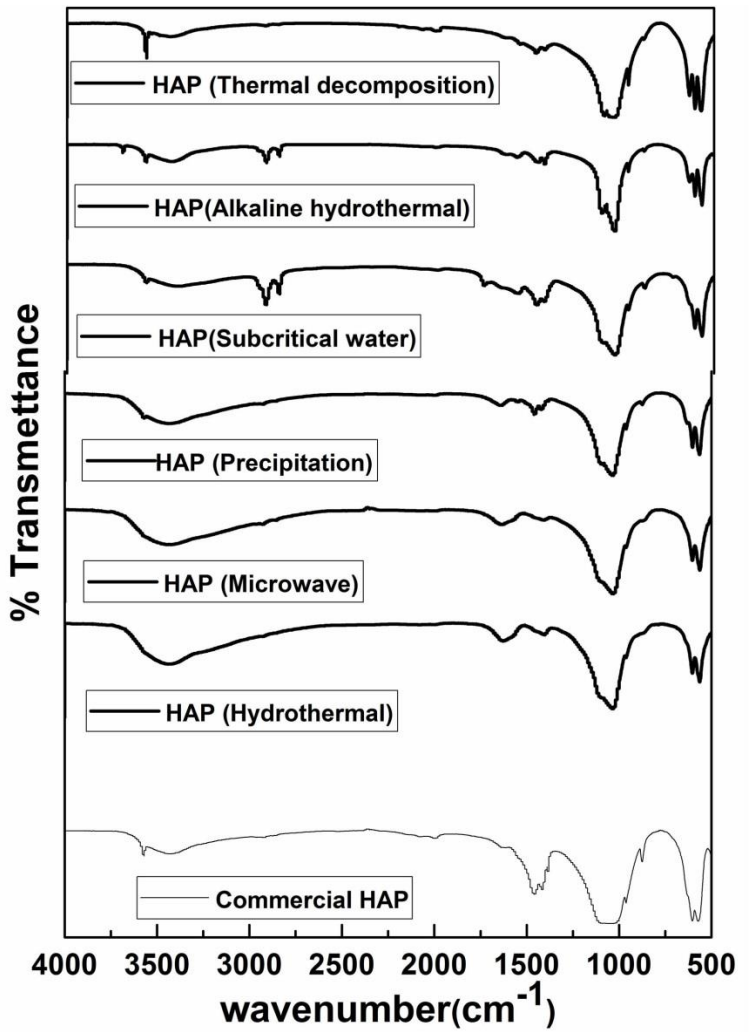

Fig. 5: FTIR spectra of the obtained HAP samples.

3.3. XPS analysis

The surface composition and stoichiometric elements of HAP were analyzed by XPS. The total spectrum and the high-energy resolution scans of the HAP produced from $CaSO_4$ extracted from CKD via microwave treatment compared with commercial HAP are depicted in Fig. 6a. Obviously, the figure shows the presence of typical elements that compose the stoichiometric ratio of Ca/P in HAP, that are, Ca 2p, P 2p and O 1s [35-37]. From XPS, the binding energies (BE) correspondents to Ca 2p3/2, P 2p and O 1s are 346.9 eV, 132.9 eV and 530.9 eV respectively. The peak corresponding to C 1s at 284.6 eV was also found and attributed to carbonate groups. Moreover, tiny amounts of other elements (Fe, Na and Mg) that rose from the inherent composition CKD were found in this sample. A high-energy resolution analysis of the individual peaks was made. The Ca 2p3/2 envelope was fitted with two peaks as observed in Fig. 6b: (i) at 346.9 eV, attributed to Ca bonds characteristic of HAP and calcium binding with carbonate due to carbon species adsorbed from air and (ii) at 344.9 eV, attributed to the presence of metallic Ca in the surface structure [38, 39]. In the Fig. 6c, the O1s envelope was fitted with three peaks centered at (i) 530.8 eV for the oxygen BE from the phosphate groups $(PO_4)^{3-}$ and OH^- groups of HAP structure, as well as $(CO_3)^{2-}$ adsorbed on HAP surface; (ii) 532.2 eV, that was attributed to oxygen atoms of adsorbed water on HAP surface and (iii) the BE of 528.8 eV that was recognized as the oxygen bonds to calcium atoms [38, 40]. The P2p envelope (Fig. 6d) was fitted with one P 2p3/2 component at 132.8 eV, which was attributed to the P-O bonds of HAP [37]. The peak fitting over the carbon C 1s region (Fig. 6e) has shown three BEs: (i) at 284.6 eV is a typical peak due to surface contamination (atmospheric organic carbon) of the type C=C and C-H bindings; (ii) at 286.5 eV attributed to C-OH and C-O-C bindings and (iii) at 289.2 eV due to C=O binding of carbonate ions adsorbed in the HAP [40, 41]. Furthermore, Table 2 depicts the atomic percentage of elements in both prepared and purchased HAP samples. The main elements (Ca, O and P) exist at high content in the following order O > Ca > P, where both contents of O and P elements are slightly higher and Ca is a little lower for the prepared HAP sample compared to purchased one. It was found that Ca/P ratio is ~ 1.66 in prepared HAP while ~ 1.76 in purchased HAP, thus the prepared HAP is better and compatible with the native ratio in naturally bone and teeth.

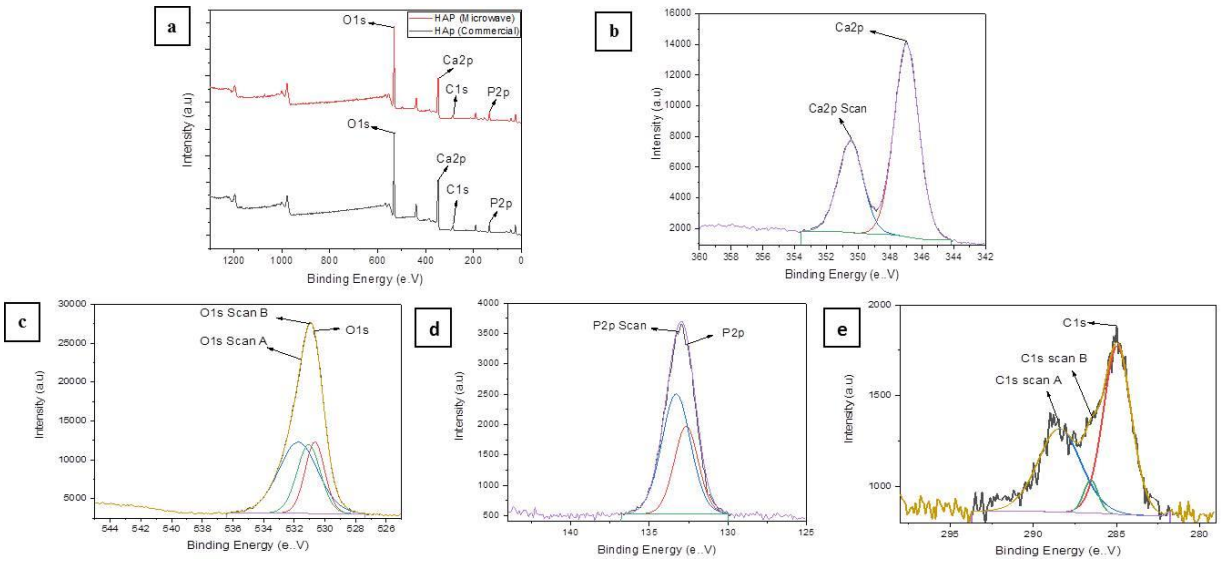

Fig. 6: XPS spectra of the HAP-microwave and commercial HAP: (a) full survey spectra, (b) Ca2p spectrum, (c) O1s spectrum, (d) P2p spectrum and (e) C1s spectrum.

Table 2: Atomic percentage for prepared HAP and purchased

Element		O1s	Ca2p	P2p	Na1s	C1s
Atomic %	**Prepared**	53.05	19.48	11.74	1.73	8.9
	Purchased	52.9	20.47	11.63	0.31	14.69

3.4. Thermal analysis

Herein, the thermal behavior of a representative HAP sample obtained from CKD-based $CaSO_4$ via microwave is recorded through thermogravimetric analysis as shown in Fig. 7. Starting from 40 °C and increasing to 800 °C, the TGA profile exhibited consecutive steps with mass loss equal to 19.32%. Additionally, a very small weight loss step between 500 and 600°C was monitored, associated with a 0.856% weight loss followed by a constant at mass loss upon 800°C. Therefore, about

~ 20% mass loss along TGA profile was obtained confirming the high thermal stability of the obtained HAP from CKD-based $CaSO_4$ by means of microwave. The corresponding DSC profile recorded for HAP revealed a series of endothermic peaks in the temperature range of 40 and 155°C, due to the slow dehydration step of the precipitated HAP, followed by a strong endothermic peak associated with the main thermal decomposition process of the prepared HAP [17].

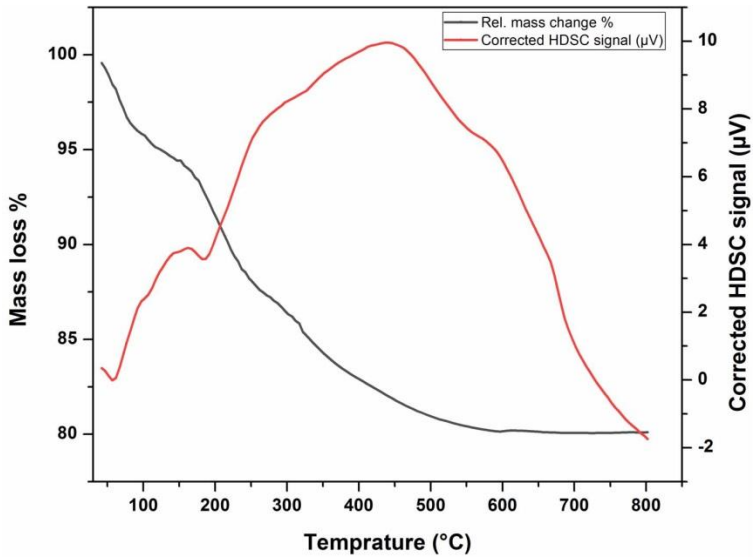

Fig. 7: TGA and DSC curves of HAP obtained from CKD-based $CaSO_4$ via microwave.

3.5. Textural analysis

Textural properties of HAP samples such as total surface area (S_{BET}, m^2/g), total pore volume (V_P, cm^3/g) and average pore radius (R_p, Å) were investigated using nitrogen adsorption/desorption isotherms as shown in Fig.8 (a and b) and listed in Table 3. The HAP samples obtained from CKD, eggshells and Buffalo bone show a type-II isotherm with an H3-hysteresis loop ($p/p^\circ > 0.6$), indicating the formation of mesoporous samples with secondary slit-shaped pores of increased size in aggregated nanoparticles [42]. The obtained HAP samples from $CaSO_4$ of CKD by microwave and hydrothermal exhibits the highest nitrogen uptake among other samples, confirming that both processes are efficient in preparing porous HAP samples, although using different calcium sources and methods. Accordingly, the total surface area values of HAP samples prepared from microwave and hydrothermal were found to be ~ 150 and 139 m^2/g with total pore volumes reached to > 0.3 cm^3/g and average pore radius > 54 Å (5.4 nm).

The corresponding pore size distributions (PSDs) calculated using the BJH method [43] from the desorption branches of these isotherms are demonstrated in Fig. 8 (c and d). In figure 8c, the applied methods (microwave, hydrothermal and precipitation) developed HAP samples with PSDs ranged between 20 – 55 Å (i.e., 2-5.5 nm), indicating the evident hierarchical mesoporous characteristics of HAP. On the other hand, HAP samples derived from Buffalo bone under different thermal processes such as subcritical water, alkaline hydrothermal and calcination, produced samples with lowest total surface areas and total pore volumes and hence lowest PSDs were developed. This result confirms that both CKD- and eggshells-based calcium sources are amenable sources to produce highly porous HAP samples rather than Buffalo bone-based calcium source. Overall, according to the textural data in Table 3, the prepared HAP in this study exhibit superior textural properties than that of purchased HAP sample.

Table 3: Textural parameters such as total surface area (S_{BET}, m^2/g), total pore volume (V_P, cm^3/g) and average pore radius (R_P, Å) of HAP obtained from different sources and methods.

Method	Calcium source	S_{BET} (m^2/g)	V_P (cm^3/g)	R_P (Å)
Purchased	Purchased sample	5	0.004	32.0
Hydrothermal	$CaSO_4$-CKD	139.6	0.307	54.9
Microwave	$CaSO_4$-CKD	150.3	0.355	54.4
Precipitation	$Ca(NO_3)_2$-eggshell	93.8	0.211	17.4
calcination	Buffalo bone	12.9	0.017	17.3
subcritical	Buffalo bone	34.0	0.055	17.3
Alkaline	Buffalo bone	16.4	0.023	17.5

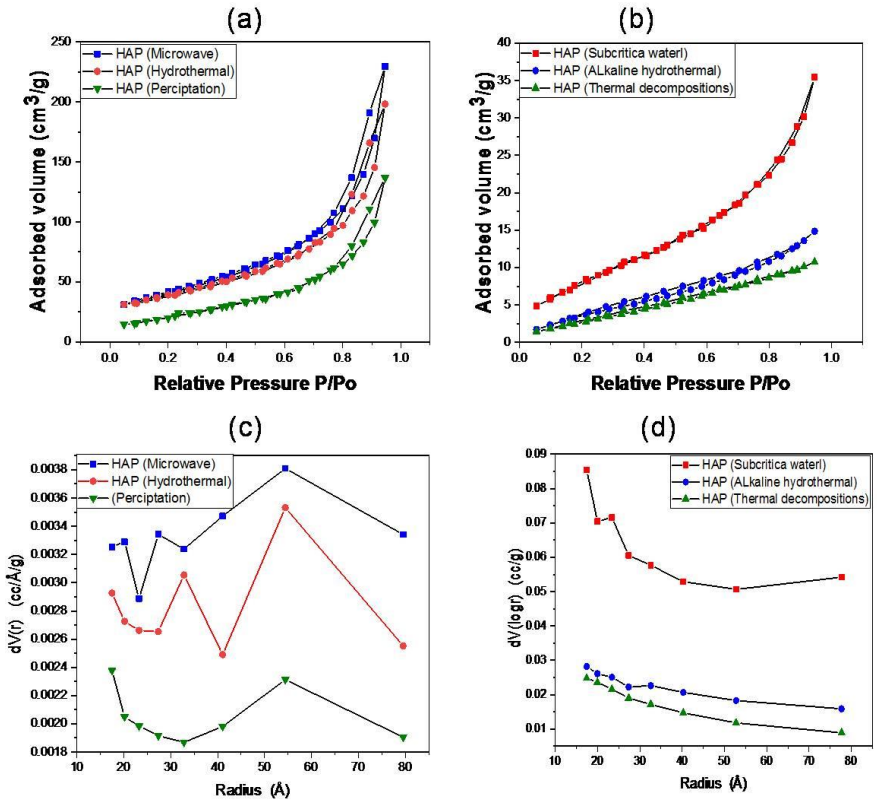

Fig. 8: (a, b) Adsorption isotherms of N_2 onto HAP samples and (c, d) their corresponding pore size distributions by BJH method.

3.6. SEM analysis

To understand the surface morphology of the prepared HAP samples, SEM images of the samples synthesized using microwave of $CaSO_4$-CKD, chemical precipitation of $Ca(NO_3)_2$-eggshell and thermal treatment of Buffalo bone at 750 ^oC for 6h are depicted in Fig. 9 (a-f) at different magnifications (x= 3500 and 5000). All samples exhibit a rough surface property. In particular, SEM images of HAP obtained from $CaSO_4$-CKD and chemical precipitation of $Ca(NO_3)_2$-eggshell showed that their surfaces composed of aggregated spherical particles which maybe organized uniformly (Fig.1 a-d). Similar results were found for HAP prepared from wet chemical precipitation of $Ca(OH)_2$ with H_3PO_4 followed by heat treatment between 100 and 800 ^oC[20, 43]. The surface of HAP derived from the thermal decomposition of Buffalo bone gives irregular spherical morphology of hydroxyapatite particles as shown in Fig 9 (e and f). Moreover, cracking with widening pores were observed on the surface of HAP-Buffalo bone through the thermal treatment performed at high temperatures, indicating the effect of thermal treatment on the surface and textural properties of obtained HAP [20, 44].

4. Conclusions

Three solid wastes of calcium-based sources have been selected for synthesizing HAP samples via different routes. Microwave, hydrothermal and wet chemical precipitation routes successfully prepared porous HAP of highly surface area from $CaSO_4$-CKD and $Ca(NO_3)_2$-eggshell. On the other hand, HAP obtained using a buffalo bone was treated with subcritical water process, alkaline hydrothermal hydrolysis and thermal decomposition exhibited lowest textural properties as well as the commercial HAP. In comparison to a commercial HAP, the results of XRD and FTIR exhibited that all prepared samples have similar crystalline phases and main functional surface groups of HAPs. In addition, XPS analysis conformed that HAP prepared through microwave of $CaSO_4$ compared to that of the commercial HAP samples contain the same specimens. Overall, the present study highlights the potential utilization of CKD- and eggshell-based calcium sources to be more suitable for producing extremely porous HAP samples than Buffalo bone-based calcium sources that are better than the commercial HAP also.

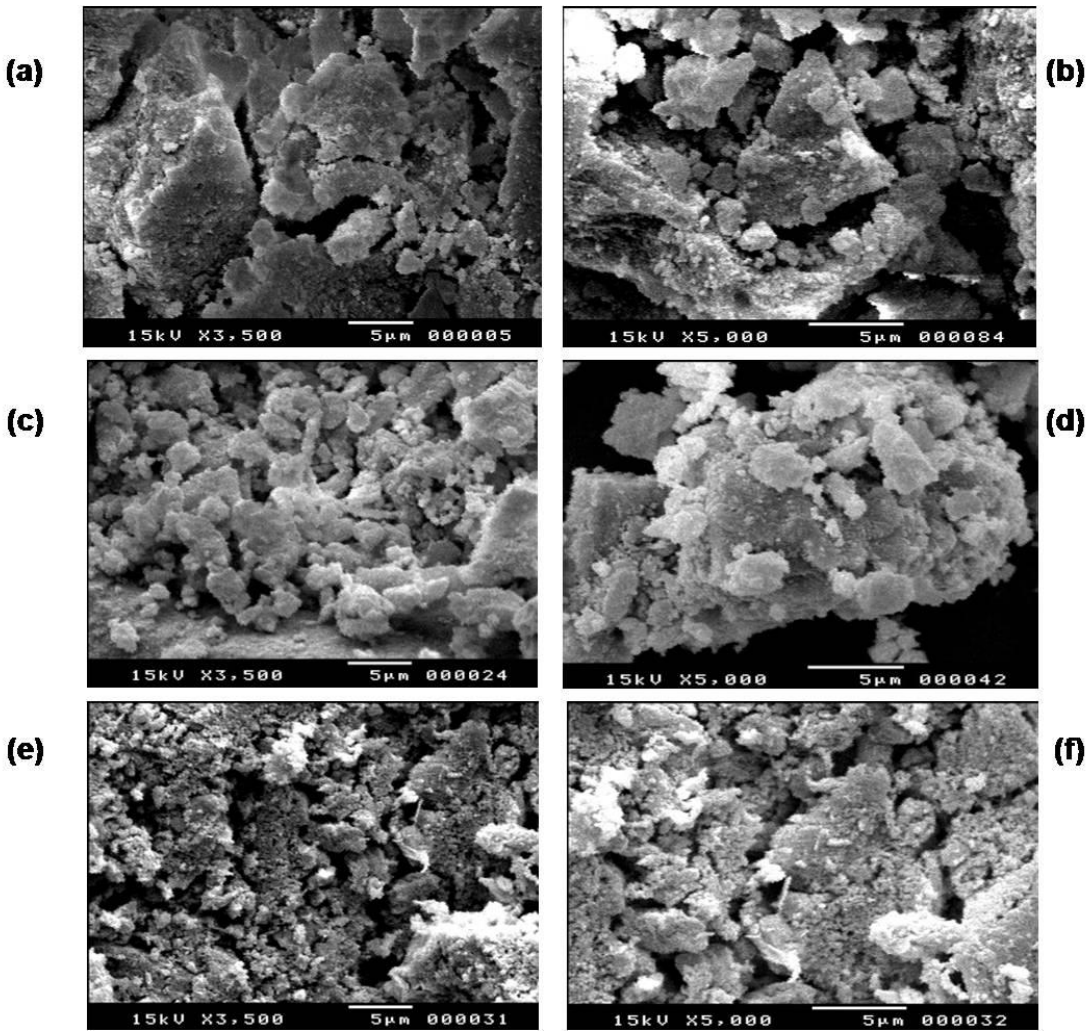

Fig. 9: SEM images of HAP samples by (a, b) microwave of $CaSO_4$-CKD, (c, d) precipitation of $Ca(NO_3)_2$-eggshell and (e, f) thermal decomposition of Buffalo bone.

Acknowledgment

The authors would like to thank the Faculty of Science, Assiut University, Egypt, for the technical and financial support.

Conflicts of interest

The authors declare that they have no known competing financial interests or personal relationships that could have appeared to influence the work reported in this paper.

Funding sources

The author(s) received no specific financial funding for this work.

References

1. P. Arokiasamy, M.M. Al Bakri Abdullah, S.Z. Abd Rahim, S. Luhar, A.V. Sandu, N.H. Jamil, M. Nabialek, Synthesis methods of hydroxyapatite from natural sources: A review, Ceramics Intern. 48 (2022) 14959-14979.

2. B.-Q. Lu, Y.-J. Zhu, One-dimensional hydroxyapatite materials: preparation and applications, Canad. J. Chem.95 (2017) 1091-1102.

3. P. Carniti, A. Gervasini, C. Tiozzo, M. Guidotti, Niobium-Containing Hydroxyapatites as Amphoteric Catalysts: Synthesis, Properties and Activity, ACS Cataly.4(2014)469-479.

4.N.A.S. Mohd Puad, P. Koshy, H.Z. Abdullah, M.I. Idris, T.C. Lee, Synthesis of hydroxyapatite from natural sources, Heliyon 5 (2019) e01588.

5. S. Mousa, N. Ammar, H. Ibrahim, Removal of lead ions using hydroxyapatite nano-material prepared from phosphogypsum waste, J. Saudi Chem. Soc. 20 (2016) 357-365.
6. A. Maidaniuc, F. Miculescu, S.I. Voicu, C. Andronescu, M. Miculescu, E. Matei, A.C. Mocanu, I. Pencea, I. Csaki, T. Machedon-Pisu, Induced wettability and surface-volume correlation of composition for bovine bone derived hydroxyapatite particles. Appl. Surf. Sci. 438(2018) 158-166.
7. Y. Chai, M. Tagaya, Simple preparation of hydroxyapatite nanostructures derived from fish scales, Materials letters 222(2018) 156-159.
8. G. Vidhya, E. Girija, Comparative study of hydroxyapatite prepared from eggshells and synthetic precursors by microwave irradiation method for medical applications, Materials Today: Proceed. 15 (2019) 344-352.
9. M. Okada, T. Matsumoto, Synthesis and modification of apatite nanoparticles for use in dental and medical applications, Jap. Dental Sci. Review 51 (2015) 85-95.
10. A. Clifford, M. Ata, I. Zhitomirsky, Synthesis, liquid–Liquid extraction and deposition of hydroxyapatite nanorod composites, Materials Lett. 201 (2017) 140-143.
11. A.A. Shaly, G.H. Priya, J.M. Linet, An outlook on the mechanical attributes and load curve analysis of hydrothermally acquired hydroxyapatite bioceramic nanoparticles, Physica B: Condensed Matter. 590(2020) 412223.
12. X. Ma, Y. Chen, J. Qian, Y. Yuan, C. Liu, Controllable synthesis of spherical hydroxyapatite nanoparticles using inverse microemulsion method, Mater. Chem. Physics 183 (2016) 220-229.
13. O. Agbabiaka, I. Oladele, A. Akinwekomi, A. Adediran, A.O. Balogun, O. Olasunkanm, T. Olayanju, Effect of calcination temperature on hydroxyapatite developed from waste poultry eggshell, Scientific African 8 (2020)1-22.
14. M. Robles-Águila, J. Reyes-Avendaño, M. Mendoza, Structural analysis of metal-doped (Mn, Fe, Co, Ni, Cu, Zn) calcium hydroxyapatite synthetized by a sol-gel microwave-assisted method, Ceramics Intern. 43(2017)12705-12709.
15. J.M.E. Drack, D.P. Vázquez, Morphological response of a cactus to cement dust pollution, Ecotox. Environ. Safety 148 (2018) 571-577.
16. M. Seo, S.-Y. Lee, C. Lee, S.-S. Cho, Recycling of cement kiln dust as a raw material for cement, Environments 6 (2019) 113.
17. M. Nasr, S.A. Halawy, S. El-Nahas, A. Abdelkader, A.I. Osman, Direct and easily prepared nanocomposite impurity-free hydroxyapatite derived from CKD as an effective catalyst for trans-2-butene production, Appl. Cataly. A: General 625(2023) 119039.
18. P. Pankaew, E. Hoonnivathana, P. Limsuwan, K. Naemchanthara, Temperature effect on calcium phosphate synthesized from chicken eggshells and ammonium phosphate, J. Appl. Sci. 10(2010) 3337-3342.
19. N. Ramesh, J.T.B. Ratnayake, S.C. Moratti, G.J. Dias, Effect of chitosan infiltration on hydroxyapatite scaffolds derived from New Zealand bovine cancellous bones for bone regeneration, Int. J. Biol. Macromol. 160(2020) 1009-1020.
20. N.A. Barakat, M.S. Khil, A. Omran, F.A. Sheikh, H.Y. Kim, Extraction of pure natural hydroxyapatite from the bovine bones bio waste by three different methods, J. Mater. Processing Technol. 209(2009) 3408-3415.
21. D.O. Obada, S.A. Osseni, H. Sina, K.A. Salami, A.N. Oyedeji, D. Dodoo-Arhin, N.D. Bansod, S. Csaki, A.Y. Atta, O.O. Fasanya, A.R. Sowunmi, L.S. Kuburi, M. Dauda, J. K. Abifarin, E.T. Dauda,Fabrication of novel kaolin-reinforced hydroxyapatite scaffolds with robust compressive strengths for bone regeneration, Appl. Clay Sci. 215 (2021) 106298.
22. M.-J. Kim, S. Jung, Calcium elution from cement kiln dust using chelating agents and CO_2 storage and $CaCO_3$ production through carbonation, Environ. Sci. Pollut. Res. 27(2020) 20490-20499.
23. K. Pavlov, B. Dmitrevskii, Influence of crystallization conditions in production of citric acid on the properties of forming calcium sulfate, Russ.J.Appl.Chem. 76(2003) 1408-1413.
24. E. Pujiyanto, P.W. Laksono, J. Triyono, Synthesis and characterization of hydroxyapatite powder from natural gypsum rock, Adv. Mater. Res. 893 (2014) 56-59.
25. O.R. Bingöl, C. Durucan, Hydrothermal synthesis of hydroxyapatite from calcium sulfate hemihydrate, Am. J. Biomed. Sci. 4(2012) 50-59.
26. M.B. Mobarak, M.S. Hossain, Z. Yeasmin, M. Mahmud, M.M. Rahman, S. Sultana, S.M. Masum, S. Ahmed, Probing the photocatalytic competency of hydroxyapatite synthesized by solid state and wet chemical precipitation method, J. Molec.Struc. 1252 (2022) 132142.
27. V. Dhand, K. Rhee, S.-J. Park, The facile and low temperature synthesis of nanophase hydroxyapatite crystals using wet chemistry, Mater. Sci. Eng.: C 36(2014) 152-159.
28. W. Khoo, F. Nor, H. Ardhyananta, D. Kurniawan, Preparation of natural hydroxyapatite from bovine femur bones using calcination at various temperatures, Procedia Manufac. 2(2015)196-201.
29. W.L. Wijesinghe, M. Mantilaka, T. Karunarathne, R. Rajapakse, Synthesis of a hydroxyapatite/poly (methyl methacrylate) nanocomposite using dolomite, Nanoscale Adv. 1(2019) 86-88.

30. M.E. Hoque, N. Sakinah, Y.L. Chuan, M. Ansari, Synthesis and characterization of hydroxyapatite bioceramic, Intern. J. Sci. Eng. Techn. 3 (2014) 458-462.
31. A.F. Ali, Z.A. Alrowaili, E.M. El-Giar, M.M. Ahmed, A.M. El-Kady, Novel green synthesis of hydroxyapatite uniform nanorods via microwave-hydrothermal route using licorice root extract as template, Ceramics Intern. 47(2021) 3928-3937.
32. A. Rodrigues, B.S. da Fonseca, A.F. Pinto, S. Piçarra, M. Montemor, Synthesis and application of hydroxyapatite nanorods for improving properties of stone consolidants, Ceramics Intern. 48(2022) 14606-14617.
33. P. Scherrer, Estimation of the Size and Internal Structure of Colloidal Particles by Means of Röntgen. Nachrichten von der Gesellschaft der Wissenschaften zu Göttingen, Math.-Phys. Kl. 2 (1918) 98-100.
34. O.A. Osuchukwu, A. Salihi, I. Abdullahi, P.O. Etinosa, D.O. Obada, A comparative study of the mechanical properties of sol-gel derived hydroxyapatite produced from a novel mixture of two natural biowastes for biomedical applications, Mater. Chem. Physics 297 (2023) 127434.
35. L. Nistor, C. Ghica, V. Teodorescu, S. Nistor, M. Dinescu, D. Matei, N. Frangis, N. Vouroutzis, C. Liutas, Deposition of hydroxyapatite thin films by Nd: YAG laser ablation: a microstructural study, Mater. Res.Bulletin 39 (2004)2089-2101.
36. J.J. Beltrano, L. Torrisi, A.M. Visco, N. Campo, E. Rapisarda, Pulsed laser deposition (PLD) technique to prepare biocompatible thin films, Adv. Sci. Techn. 49(2006) 56-61.
37. E. Mavropoulos, M. Hausen, A.M. Costa, G. Alves, A. Mello, C. Ospina, M. Mir, J.M. Granjeiro, A.M. Rossi, The impact of the RGD peptide on osteoblast adhesion and spreading on zinc-substituted hydroxyapatite surface, J. Mater. Sci.: Mater. Medicine 24 (2013) 1271-1283
38. T. Hanawa, M. Ota, Calcium phosphate naturally formed on titanium in electrolyte solution, Biomaterials12 (1991) 767-774.
39. S. Kačiulis, G. Mattogno, L. Pandolfi, M. Cavalli, G. Gnappi, A. Montenero, XPS study of apatite-based coatings prepared by sol–gel technique, Appl. Surf. Sci. 151 (1999) 1-5.
40. B. Demri, D. Muster, XPS study of some calcium compounds, J. Mater. Processing Techn. 55 (1995) 311-314.
41. C.D. Wagner, Handbook of X-ray photoelectron spectroscopy: A reference book of standard data for use in X-ray photoelectron spectroscopy, Editor: G. E. Muilenberg, Perkin-Elmer (1979).
42. X. Li, D. Zeng, L. Chen, P. Ke, Y. Tian, G. Wang, Preparation and characterization of magnetic chitosan hydroxyapatite nanoparticles for protein drug delivery and antibacterial activity, J. Mater. Res. 36 (2021) 4307-4316.
43. J. Rouquerol, D. Avnir, C.W. Fairbridge, D.H. Everett, J. Haynes, N. Pernicone, J.D. Ramsay, K.S.W. Sing, K.K. Unger, Recommendations for the characterization of porous solids (Technical Report). Pure Appl. Chem.66 (1994) 1739-1758.
44. Y. Han, S. Li, X. Wang, L. Jia, J. He, Preparation of hydroxyapatite rod-like crystals by protein precursor method, Mate. Res.Bulletin 42(2007) 1169-1177.